Estimation and Compensation of Doppler Scale in UAC OFDM Systems

Sadia Ahmed

Department of Electrical Engineering
University of South Florida
Email: ahmed3@mail.usf.edu

***Abstract*—Doppler effect causes loss of orthogonality in Orthogonal Frequency Division Multiplexing (OFDM), which in turn may severely degrade receiver performance. In high data rate underwater acoustic communication (UAC), the effect of Doppler shift varies considerably over OFDM frequency band. In the past and current UAC OFDM literature [1]- [6], the frequency domain Doppler shift is presented in terms of path dependent Doppler scale in time domain. This paper proposes and presents two algorithms to estimate Doppler scale induced by time variability of the channel. The performance of these estimation methods is evaluated under varying sampling period, varying number of channel taps, and varying channels.**

I. Problem with Varying Doppler Shift in UAC OFDM Systems

In underwater acoustic communication (UAC) channel, Doppler causes significant degradation in transmission. According to the literature [7], [8], the two Doppler effects, shift and spread, are caused by two different sources. The *Doppler shift* is a function of the relative velocity of the transducers/hydrophones and other objects, variable acoustic velocity, and signal frequencies. The *Doppler spread* on the other hand, is primarily caused by the wind speed on the surface waves and by the internal currents. The total Doppler effect is a combination of Doppler shift and Doppler spread, where the average Doppler shift is much larger compared to overall Doppler spread [8].

In OFDM systems Doppler causes loss of orthogonality. This in turn may severely degrade receiver performance. In underwater OFDM, the bandpass frequency is comparable (for example, in Hz or kHz) to the baseband subcarrier frequencies (for example, in Hz or kHz). In such cases, the individual subcarrier frequency variation from the bandpass frequency is significant. Therefore, the effect of Doppler shift on OFDM signal will vary over subcarriers. The shift on the kth subcarrier due to the mth scatterer in baseband OFDM can be expressed as,

$$F_{Dkm} = \frac{v_w}{c_w} f_k cos\theta_m \ , \qquad (1)$$

where f_k is the kth subcarrier frequency, θ_m is the scattering angle of the mth scatterer, c_w is the sound speed in water, and v_w is the mobile velocity in water. Compared to the narrowband terrestrial RF, Doppler shift effect in UAC is more severe over OFDM subcarriers. This is primarily due to, A) Very low acoustic velocity compared to RF velocity, c_a i.e. $c_w << c_a$) giving rise to high Doppler shift effect, B) The comparable Doppler amount to the low values of

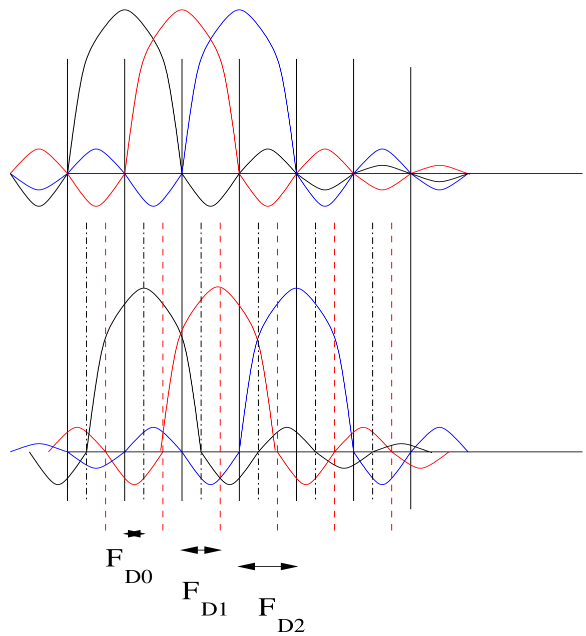

Fig. 1: Varying Effect of Doppler Shift over OFDM Subcarriers

subcarrier frequencies effect each subcarrier, and C) The variable Doppler shift effect over subcarriers due to low bandpass frequencies. Fig. 1 illustrates the varying effect of Doppler shift over OFDM subcarriers. In this paper, two methods of time domain estimation of Doppler scale are proposed. The performance of these estimation methods is evaluated under varying sampling period, varying number of channel taps, and varying channels. The contribution of this paper are listed below.

- Two Doppler scale estimation methods are proposed to estimate the Doppler scale in time domain that causes Doppler shift over OFDM subcarriers in frequency domain. In both methods, at the transmitter, a known reference OFDM symbol is transmitted prior to transmitting data OFDM symbols. At the receiver, the received reference symbol, which is convolved with the channel, is cross-correlated at different delays, with the local known symbol, provided by the receiver that has not been convolved with the channel. The correlation operation determines the channel tap positions. In the first method, channel tap positions in the absence of Doppler are

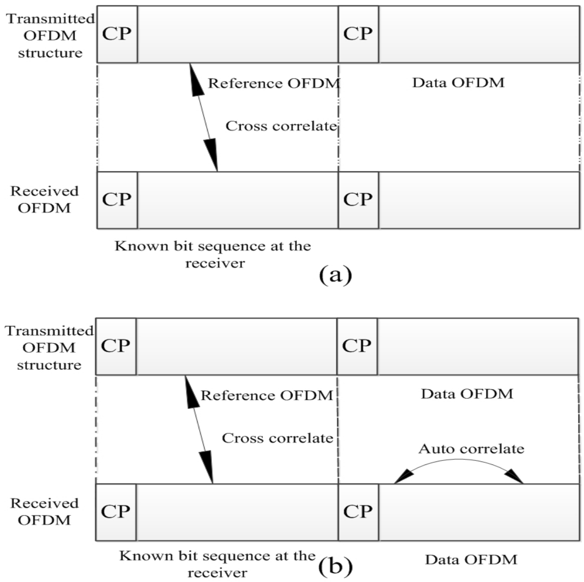

Fig. 2: Signal Structure, Doppler Scale Estimation Methods

assumed *known*. The tap positions in the presence and in the absence of Doppler are compared to estimate the Doppler scale. In the second method, the channel tap positions in the absence of Doppler are *unknown* and a data OFDM symbol is auto-correlated at the receiver. The tap positions within the cross correlated reference and auto correlated data OFDM symbols are compared to determine the Doppler scale. Fig. 2 (a) illustrates the first method and Fig. 2 (b) illustrates the second method.

- Analysis of the two methods are derived. Simulation results are provided.

The rest of the paper is organized as follows. In Section II, a brief literature study is presented on Doppler effect in underwater acoustic OFDM. In Section III, the proposed algorithms to estimate Doppler scale are presented. In Section IV, the analysis of Doppler effect is presented. In Section V, the simulation results are provided for both the algorithms. In Section VI, the concluding remarks are presented.

II. Related Work on Doppler Shift in UAC OFDM

In [9], an iterative receiver is proposed to estimate Doppler and channel parameters and decode in an iterative manner where previous iteration values are used to compute future estimations. In [10], Doppler is treated as carrier frequency offset (CFO) and the CFO is estimated in an iterative manner. In this paper, the proposed Doppler scale estimation methods do not treat Doppler as CFO. Doppler scale results from time variability of the UAC channel and therefore, is not fixed over time. In the proposed methods, no previous estimated values are used in future estimations.

In [11], an adaptive frequency domain equalizer is utilized in coded OFDM. In [12], oversampling is done in frequency domain to mitigate Doppler effect. In this paper, the proposed estimation methods conduct the estimation, resampling, and compensation in time domain.

In [13], two ICI mitigation techniques are proposed. In the first method, ICI is explicitly estimated and in the second, instead of determining ICI values detection is done by adaptive decision feedback equalization. In [14], a factor graph based equalization method is utilized to mitigate both ICI and inter block interference (IBI). In this paper, the proposed Doppler scale estimation and compensation are conducted in time domain. No ICI values or its components are determined.

In [15], adaptive detection method is proposed in MIMO OFDM signals to compensate non-uniform Doppler. In [16], a multiband OFDM is utilized to tackle Doppler. In this paper, the Doppler scale estimation methods are proposed for single band OFDM systems.

In [2]- [5] a Doppler rate factor is determined to estimate Doppler and is compensated in the time domain. Similar to these publications, the two proposed Doppler estimation methods in this paper estimate Doppler scale in time domain. However, in the prior publications, two extra identical OFDM symbols are transmitted prior to transmitting the data OFDM symbols. At the receiver, these two transmitted symbols are correlated to determine the Doppler scale. In other cases, a preamble and a postamble are transmitted with the OFDM block. By comparing the length of the received OFDM block with the expected length, the Doppler scale is determined. In this paper, in the proposed Doppler scale estimation methods, one reference OFDM symbol is transmitted prior to data OFDM block. This reference OFDM is used with a local known symbol at the receiver to estimate Doppler scale in the first method. In the second proposed method, one data OFDM symbol is used in addition to estimate Doppler scale.

In [17], [18], the bounds of optimal resampling factor is determined when the Doppler scale varies over taps. In this paper two Doppler scale estimation methods are proposed to estimate Doppler scale, when the scale is non-varying over taps and when it is varying. No optimal resampling factor is derived.

III. Proposed Estimation Techniques

The proposed Doppler scale estimation algorithms operate in time domain. Fig. 2 illustrates the signal structure for both algorithms. In both methods a known OFDM reference symbol is transmitted prior to transmitting the data symbols. This reference is cross correlated with the local known symbol at the receiver.

In the second proposed method, in addition to the reference cross-correlation, a data OFDM symbol is autocorrelated. In Fig. 3, the reference OFDM symbol is shown preceding the data OFDM block at the end of the IFFT operation. Fig. 4 (a) illustrates the receiver architecture for the first algorithms and Fig. 4 (b) for the second. The rest of this section presents the two methods.

A. First Estimation Algorithm

The estimation algorithm is presented below.

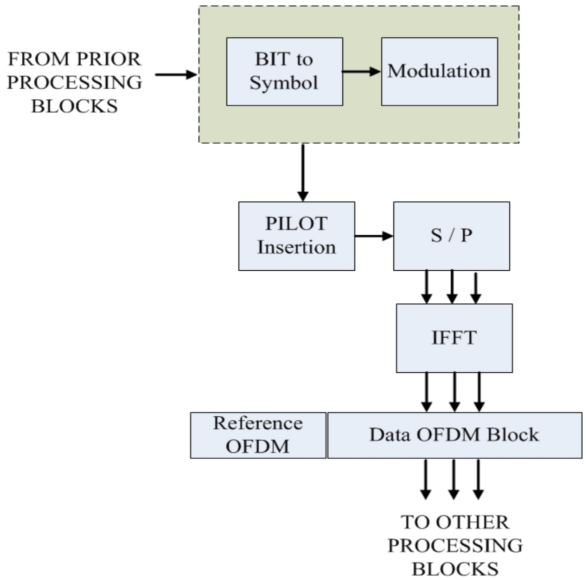

Fig. 3: Transmitter Block Diagram

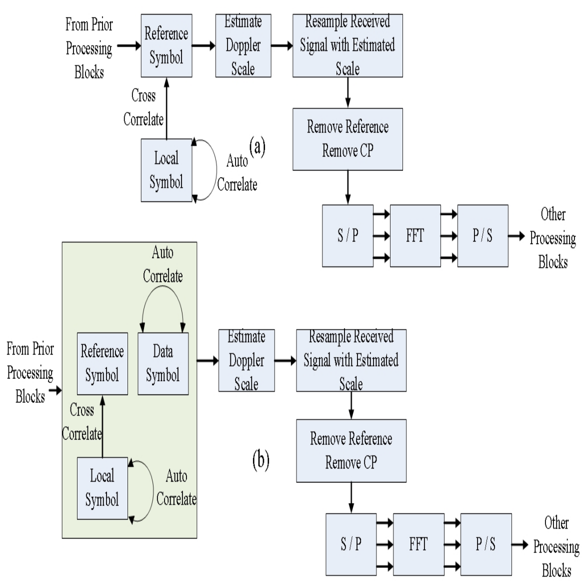

Fig. 4: Receiver Block Diagram

- Cross correlate received reference symbol with the local known OFDM symbol.
- Determine the peak location/s.
- Compare each peak location with the corresponding known peak location. The difference determines the Doppler scale.

In the scenario, where the Doppler scale is assumed to be same on all taps, the scale is averaged over multiple peak differences. When the scale varies over taps, each peak will correspond to each path dependent Doppler scale.

B. *Second Estimation Algorithm*

In the second estimation method, in addition to the reference symbol, an OFDM data symbol is auto correlated. The algorithm is described below:

- Cross correlate received reference symbol with the local known OFDM symbol.
- Determine the peak location/s.
- Auto correlate the successive data OFDM symbol. Determing the peak location/s.
- Compare the peak location within the reference with the corresponding peak location within the data OFDM. The difference in peak location pairs determines the Doppler scale.

IV. Analysis of Time Varying Channel in UAC OFDM Systems

A frequency selective and time varying channel can be expressed as [19],

$$h(t, \tau_{REF}) = \sum_{l=0}^{L-1} \alpha_l(t, \tau_{REF}) \delta(\tau_{REF} - \tau_l(t)), \qquad (2)$$

where $\alpha_l(t, \tau)$ and $\tau_l(t)$ represent time varying attenuation coefficient and time varying tap delay of the lth delay bin respectively. Both parameters are function of time and depend on the scatterers arriving within the lth bin. The variable L represents the total number of multipaths or delay bins and δ represents the Dirac Delta function. In discrete domain (2) can be expressed as,

$$\begin{aligned} h(n, nT_s) &= \sum_{l=0}^{L-1} \alpha_l(n, nTs) \delta(nT_s - \tau_l(n)) \\ &= \sum_{l=0}^{L-1} h_l(n), \\ &= h_0(n) + h_1(n) + h_2(n) + ..., \end{aligned} \qquad (3)$$

where variable T_s denotes the sampling period, nT_s represents the time corresponding to the nth sample. The channel impulse $h(n)$ is a complex quantity. It can be assumed that the real and imaginary components of $h(n)$ are independent and identically distributed (i.i.d.) and follow Gaussian distribution. Under such condition, the modulus of $h(n)$ or $|h(n)|$ will follow Rayleigh distribution [19]. Each scatterer causes a Doppler shift while M scatterers arriving at the same instance within the delay bin will cause Doppler spread.

The Doppler shift in frequency domain is caused by both time varying attenuation and time varying delay of each tap as seen in (3). In accordance to the literature in UAC, the time varying delay in time domain is considered to be the primary cause of Doppler shift in frequency domain. The time variability of each delay bin can be quantified with a scale factor known as Doppler scale.

In the rest of this section, first the general analysis is presented. Then individual analysis for each estimation method is presented. The following assumptions are made for simplicity of analysis,

- Each individual channel scatter within a channel tap, ideally, is associated with an attenuation, a delay, and a Doppler scale. It is reasonably assumed that all scatters within a channel tap have same delay, and Doppler scale, but different attenuation.
- It is reasonably assumed that channel tap attenuation, time invariant part of the delay, and Doppler scale parameter remain same over a block of OFDM symbols.
- The Doppler scale is first assumed to be same over all channel taps. This assumption is later removed.
- The tap attenuation is invariant over time, i.e. $\alpha_l(n) \approx \alpha_l$.

The time varying delay, $\tau_l(n)$ can be expressed as

$$\begin{aligned} \tau_l(n) &= \tau_l - an \\ \tau_l(n) &= lT_s - alT_s, \end{aligned} \tag{4}$$

where a denotes the Doppler scale. In a frequency selective and fast fading channel, the kth channel frequency sample using (3) and (4) , can be expressed as,

$$\begin{aligned} H_k(n) &= \sum_{l=0}^{L-1} h_l(n) e^{-j2\pi f_k n} \\ &= \sum_{l=0}^{L-1} h_l e^{-j2\pi f_k \tau_l} e^{j2\pi f_k a n} \end{aligned} \tag{5}$$

The *OFDM signal structure* is represented as follows. After performing inverse fast Fourier transform (IFFT) on the frequency domain OFDM symbol, the nth discrete time sample of the transmitted OFDM symbol can be expressed as,

$$X_n = \sum_{k=0}^{N-1} X_k e^{j2\pi \frac{nk}{N}} \quad 0 \leq n \leq N-1, \tag{6}$$

where N is the total number of FFT points. Replacing nk/N in (6),

$$\begin{aligned} X_n &= \sum_{k=0}^{N-1} X_k e^{j2\pi f_k (nT_s)} \quad 0 \leq n \leq N-1, \\ &= \sum_{k=0}^{N-1} X_k e^{j2\pi f_k (n)} \quad 0 \leq n \leq N-1, \end{aligned} \tag{7}$$

where the real and imaginary components of the complex sample X_n are assumed to be i.i.d. Gaussian distributed [20]. If the channel is frequency selective, an additional cyclic prefix (CP) of length G will be added to each OFDM symbol such that, $G \geq M$. The sample of the transmitted OFDM symbol with CP can be expressed as (similar to [21]),

$$X'_n = \begin{cases} X_n & 0 \leq n \leq N-1 \\ X_{N+n} & -G \leq n \leq -1 \end{cases}$$

After the removal of the cyclic prefix, the above equation deduces to (7).

The *received OFDM signal* is expressed as follows. In a frequency selective and a fast fading channel, the received OFDM symbol can be expressed as a discrete convolution between the transmitted symbol and the channel (similar to [21], [22]). Then the nth time sample Y_n of the recieved symbol is,

$$\begin{aligned} Y_n &= \sum_{l=0}^{L-1} h_l(n) X_{n-l} \quad 0 \leq n \leq N-1, \\ &= h_0(n)X_n + h_1(n)X_{n-1} + h_2(n)X_{n-2}... \end{aligned} \tag{8}$$

where the n in $h_l(n)$ denotes the time variation of the lth tap or bin. After performing fast Fourier transform (FFT) on the time domain received symbol, the frequency domain kth sample can be expressed as, $Y_k = \frac{1}{N}\sum_{n=0}^{N-1} Y_n e^{-j2\pi\frac{nk}{N}} = \frac{1}{N}\sum_{n=0}^{N-1} Y_n e^{-j2\pi f_k n}$. Using (8),

$$Y_k = \frac{1}{N}\sum_{n=0}^{N-1}\Big[\sum_{l=0}^{L-1} h_l(n) X_{n-l}\Big] e^{-j2\pi f_k n}. \tag{9}$$

$$h_l(n) = \alpha_l \delta(nT_s - (\tau_l - an)). \tag{10}$$

When the Doppler scale varies over channel taps, i.e. each channel tap is associated with a different Doppler scale, eqn. (10) becomes

$$h_l(n) = \alpha_l \delta(nT_s - (\tau_l - a_l n)), \tag{11}$$

where a_l denotes the Doppler scale specific to lth tap delay. The received reference symbol, after convolving with the time varying channel, using (8) and (10) can be expressed as,

$$Y[n] = h_0 X_{n-an} + h_1 X_{n-1-an} + h_2 X_{n-2-an} + ..., \tag{12}$$

where X_{n-an} are known values at the receiver and the time variation of tap delays correspond to the convolution of channel taps with samples at time variant sample locations. When Doppler scale varies per channel taps, eqn. (12) becomes,

$$Y[n] = h_0 X_{n-a_0 n} + h_1 X_{n-1-a_1 n} + h_2 X_{n-2-a_2 n} + ... \tag{13}$$

In the *First Estimation Method*, as presented in section III, applying the Doppler scale estimation algorithm, the correlation operation at different lags between the received reference and the local known clean OFDM symbol, can be expressed as (using eqn. (12)),

$$\begin{aligned} RR_D[an] &= E[Y[n] * X[n-an]] \\ &= h_0 |X_{n(1-a)}|^2 + 0..., \\ &= PR_{D0} + 0... \\ RR_D[an-1] &= E[Y[n] * X[n-an-1] \\ &= h_1 |X_{n(1-a)-1}|^2 + 0 \\ &= PR_{D1} + 0... \end{aligned} \tag{14}$$

Using eqn. (14), each tap value can be determined by,

$$|h_l| = \frac{PR_{Dl}}{|X_{n(1-a)-l}|^2}, \tag{15}$$

Using eqn. (14), each tap location within the reference OFDM symbol in the presence of Doppler can be determined by,

$$[n_{R_{D1}}] = \arg\max RR_D[n] \tag{16}$$

$$[n_{R_{D2}}] = \arg\max RR_D[n], n \neq PRL_{D1}, \tag{17}$$

$$[n_{R_{D3}}] = \arg\max RR_D[n], n \neq PRL_{D1}, n \neq PRL_{D2}, \tag{18}$$

where each peak location, in terms of sample index, $PRL_{D1} = [n_{R_{D1}}]$, $PRL_{D2} = [n_{R_{D2}}]$, $PRL_{D3} = [n_{R_{D3}}]$ gives the time variant sample location after Doppler displacement of each tap. This location is compared with the known tap location in the absence of Doppler to estimate Doppler scale. Let the peak locations in the absense of Doppler be denoted as, PL_{ND1}, PL_{ND2}, PL_{ND3} etc. Then the Doppler scale a_r can be determined using eqn. (18) as follows,

$$\begin{aligned} \hat{a_r} &= \frac{PL_{ND1} - PRL_{D1}}{n_{ND1}}, \\ \hat{a_r} &= \frac{n_{ND1} - n_{ND1} + a_r n_{ND1}}{n_{ND1}}, \end{aligned} \tag{19}$$

where n_{NDi} denotes the sample location of the peak in the absence of Doppler. Averaging over all taps, using eqn. (19), the estimated Doppler scale becomes,

$$\hat{a_r} = \frac{1}{L}\sum_{i=0}^{L-1} \frac{a_{r_i} n_{NDi}}{n_{NDi}} \tag{20}$$

When Doppler scale is variable over taps, by considering multiple peaks for multiple taps and their corresponding sample locations, the tap/path dependent Doppler scales, a_{rl} can be estimated.

If the actual Doppler scale is denoted by a, then the difference between actual and estimated scale can be determined by,

$$\begin{aligned} a - \hat{a_r} &= a - \frac{1}{L} a_r \sum_{i=0}^{L-1} \frac{n_{NDi}}{n_{NDi}} \\ &= a - \hat{a_r}\beta \end{aligned} \tag{21}$$

Therefore, the estimated scale will be equal to the actual a if β in the second term in (21) is equal to 1. From (21), the following can be stated,

- the estimation accuracy is a function of number of taps. More number of taps can also imply the accuracy will be more prone to noise from each tap.
- Since the location of correlated peaks is used in estimation, the higher the values of taps, the more accurate will be the estimation.
- the estimation accuracy depends on the known code sequence used. In other words the reference symbol must possess strong autocorrelation property such that (14) yields a 0 at cross correlated positions. To express this (14) can be modified to have,

$$\begin{aligned} RR_D[an] &= E[Y[n] * X[n - an]] \\ &= P_{D0} + \epsilon ... \\ RR_D[an-1] &= E[Y[n] * X[n - an - 1] \\ &= P_{D1} + \epsilon ..., \end{aligned} \tag{22}$$

  then $\epsilon = 0$. The noise present in the received reference symbol will contribute to noise in the cross correlated peaks.

In the *Second Proposed Estimation Method*, a data OFDM is auto correlated in addition to the operations on the reference OFDM in the first method. The auto correlated peaks within the data OFDM, PD_{Di}s can be expressed as,

$$\begin{aligned} RD_D[0] &= E[Y[n] * Y[n]] \\ &= h_0^2 |X_{n(1-a)}|^2 + h_1^2 |X_{n(1-a)-1}|^2 \\ &\quad + h_2^2 |X_{n(1-a)-2}|^2 ..., \end{aligned}$$

$$RD_D[0] = PD_{D0} + PD_{D1} + PD_{D2} + ... \tag{23}$$

Using eqn. (23), each tap location within the data OFDM symbol in the presence of Doppler can be determined by,

$$[n_{D_{D1}}] = \arg\max RD_D[n] \tag{24}$$

$$[n_{D_{D2}}] = \arg\max RD_D[n], n \neq PDL_{D1}, \tag{25}$$

$$[n_{D_{D3}}] = \arg\max RD_D[n], n \neq PDL_{D1}, n \neq PDL_{D2}, \tag{26}$$

where each peak location, $PDL_{D1} = [n_{D_{D1}}]$, $PDL_{D2} = [n_{D_{D2}}]$, $PDL_{D3} = [n_{D_{D3}}]$ gives the time variant sample location after Doppler displacement of each tap within the data OFDM. This location is compared with the tap locations in the cross correlated reference OFDM found in equations, (18). Then the Doppler scale a_{RD} can be determined using eqn. (18) and (26) as follows,

$$\begin{aligned} PRL_{D0} - PDL_{D0} &= n_{R_{D0}} - n_{D_{D0}} \\ &= T_{OFDM} + \hat{a_{rD}} n_{ND0} \end{aligned}$$

$$\begin{aligned} \hat{a_{rd}} &= \frac{n_{R_{D0}} - n_{D_{D0}} - T_{OFDM}}{n_{ND0}} \\ \hat{a_{rd}} &= \frac{(n_{R_{D0}} - n_{D_{D0}}) - N}{n_{ND0}} \end{aligned} \tag{27}$$

Averaging over all taps, using eqn. (27), the estimated Doppler scale becomes,

$$\hat{a_{rd}} = \frac{1}{L}\sum_{i=0}^{L-1} \frac{(n_{R_{Di}} - n_{D_{Di}}) - N}{n_{NDi}} \tag{28}$$

The noise present in the received reference and data symbols will contribute to noise in the cross correlated peaks and auto correlated peaks respectively. When Doppler scale is variable over taps, by considering multiple peaks for multiple taps and their corresponding sample locations, the tap/path dependent Doppler scales, a_{rd_l} can be estimated.

If the actual Doppler scale is denoted by a, then the difference between actual and estimated scale can be determined by,

$$a - \hat{a_{rd}} = a - \frac{1}{L}\sum_{i=0}^{L-1} \frac{(n_{R_{Di}} - n_{D_{Di}}) - N}{n_{NDi}} \tag{29}$$

Therefore, the estimated scale will be equal to the actual a if the second term in (29) is equal to 0. The same three statements derived from (21) can be stated for (29) with the addition that the data sequence in the data OFDM may need to have good autocorrelation property as well.

In both of the proposed methods, in order to accurately estimate Doppler scale, the sampling period needs to be carefully chosen such that, either a_r or a_{rd} is a multiple of the sampling period,

$$\begin{aligned} a_r &= mT_s, \\ a_{rd} &= mT_s, \end{aligned} \tag{30}$$

where m denotes a fraction multiple.

The *ICI and SIR* can be expressed as follows. Using (6) in (9),

$$Y_k = \frac{1}{N}\sum_{n=0}^{N-1}\underbrace{\Big[\sum_{l=0}^{L-1} h_l(n)\Big(\sum_{k=0}^{N-1} X_k e^{j2\pi f_k(n-l)}\Big)\Big]}_{A_k} \cdot e^{-j2\pi f_k n}. \tag{31}$$

The A_k of (31) can be expanded using (5) and is expressed as below,

$$\begin{aligned}
&= \Big[\sum_{l=0}^{L-1} h_l(n)\Big(X_k e^{j2\pi f_k(n-l)} + \sum_{p=0,p\neq k}^{N-1} X_p e^{j2\pi(n-l)f_p}\Big)\Big] \\
&= \Big[X_k \sum_{l=0}^{L-1} h_l(n) e^{j2\pi(n-l)f_k} \\
&+ \sum_{p=0,p\neq k}^{N-1} X_p \sum_{l=0}^{L-1} h_l(n) e^{j2\pi(n-l)f_p}\Big] \\
&= \Big[\Big(X_k \sum_{l=0}^{L-1} h_l(n).e^{-j2\pi f_k l}\cdot e^{j2\pi f_k n}\Big) \\
&+ \Big(\sum_{p=0,p\neq k}^{N-1} X_p \sum_{l=0}^{L-1} h_l(n) e^{-j2\pi f_p l}\cdot e^{j2\pi f_p n}\Big)\Big] \\
&= \Big[\Big(e^{j2\pi f_k n} X_k \sum_{l=0}^{L-1} h_l(n) e^{-j2\pi f_k l}\Big) \\
&+ \Big(\sum_{p=0,p\neq k}^{N-1} X_p \sum_{l=0}^{L-1} h_l(n) e^{-j2\pi f_p l} e^{j2\pi f_p n}\Big)\Big] \\
&= \Big[e^{j2\pi f_k n} X_k H_k(n) + e^{j2\pi f_p n}\sum_{p=0,p\neq k}^{N-1} X_p H_p(n)\Big]
\end{aligned} \tag{32}$$

Using the value of A from (32) in(31) and after some simple computation, the received signal can be expressed as,

$$\begin{aligned}
Y_k &= \underbrace{\frac{1}{N}\sum_{n=0}^{N-1} X_k H_k(n)}_{Desired} \\
&+ \underbrace{\frac{1}{N}\sum_{n=0}^{N-1}\sum_{p=0,p\neq k}^{N-1} X_p H_p(n) e^{j2\pi n(f_k - f_p)}}_{ICI}, \\
&= \underbrace{\frac{1}{N}\sum_{n=0}^{N-1} X_k H_k(n)}_{Desired} \\
&+ \underbrace{\frac{1}{N}\sum_{n=0}^{N-1}\sum_{p=0,p\neq k}^{N-1} X_p H_p(n) e^{j2\pi n\Delta f(p-k)}}_{ICI}
\end{aligned} \tag{33}$$

where both the desired and the ICI are complex values incorporating time varying channel, where n denotes the time variability. The time variation of each tap is expressed as time variation of the delays in terms of Doppler scale. Using (5) in (33) the desired signal can be expressed as,

$$D_{NC} = \frac{1}{N}\sum_{n=0}^{N-1} X_k \sum_{l=0}^{L-1} h_l e^{-j2\pi f_k l T_s(1+a)}, \tag{34}$$

$$D_C = \frac{1}{N}\sum_{n=0}^{N-1} X_k \sum_{l=0}^{L-1} h_l e^{-j2\pi f_k l T_s \frac{(1+a)}{(1+\hat{a})}}, \tag{35}$$

where D_{NC} and D_C denote the desired signal part without and with Doppler compensation respectively. The symbol, $\hat{a}$ is the general Doppler scale and can be estimated using either of the two proposed methods. Using (5) in (33) the ICI part can be expressed as,

$$\begin{aligned} ICI_{NC} &= \frac{1}{N}\sum_{n=0}^{N-1}\sum_{p=0,p\neq k}^{N-1} X_p e^{j2\pi n\Delta f(p-k)} \\ &\cdot \sum_{l=0}^{L-1} h_l e^{-j2\pi f_k l T_s(1+a)}, \end{aligned} \tag{36}$$

$$\begin{aligned} ICI_C &= \sum_{n=0}^{N-1}\sum_{p=0,p\neq k}^{N-1} X_p e^{j2\pi n\Delta f(p-k)} \\ &\cdot \sum_{l=0}^{L-1} h_l e^{-j2\pi f_k l T_s \frac{(1+a)}{1+\hat{a}}}, \end{aligned} \tag{37}$$

where ICI_{NC} and ICI_C denote the ICI components in the absense and in the presence of Doppler effect respectively.

When Doppler scale is estimated accurately, i.e. $\frac{(1+a)}{(1+\hat{a})} \approx 1$ in (35) and in (37), there will be no contribution of time varying effect into the desired signal part and into the ICI part respectively. Taking into account an additive white Gaussian noise (AWGN) term with zero mean and variance of σ_n, the signal to interference plus noise ratio (SINR) can be expressed as,

$$\begin{aligned} SINR_{ICI} &= \frac{Signalpower}{ICIpower + noisepower} \\ &= \frac{E|Desired|^2}{E|ICI|^2 + \sigma_n}, \end{aligned} \tag{38}$$

V. Simulation Results

The simulation is carried out using the parameters in Table I. The results are provided for realistic underwater acoustic channel responses provided in [23]. The simulation is carried out for various SNR values. The following two sub sections discuss the simulation results for the two estimation methods.

TABLE I: Doppler Shift Simulation Parameters

Parameters	Values
FFT Size	256
Carrier Frequency(kHz)	60
Bandwidth(kHz)	40
Number of taps	1,3
Channel(m)	100,50
Sampling rate (times)	10,50,1000
TxRx Speed(m/sec)	$[.01 : .1 : 3]$
Signal Velocity(m/sec)	1350
Realizations	10000
Channel	Actual

A. Simulation Using First Algorithm

Fig. 5 and 6 illustrates the coarse estimated Doppler scale in a 100m channel using the first 3 channel taps for 10 times and 50 times the original sampling rate respectively. The estimated Doppler scale values are more scattered with sampling rate of 10 compared to 50. Fig. 7 and 8 illustrates the coarse estimated Doppler scale in a 100m channel using only the first channel tap for 10 times and 50 times the original sampling rate respectively. The estimated Doppler scale values are more scattered with sampling rate of 10 compared to 50.

Ideally, estimation with 3 taps should provide better accuracy. At the same time higher number of taps inject more noise in the estimation calculation. In the above figures it can be seen that compared to estimation with 3 taps, estimation with 1 tap gives less scattered values in both sampling rate situations.

Fig. 9 and 10 illustrates the coarse estimated Doppler scale in a 50m channel using the first 3 channel taps for 10 times and 50 times the original sampling rate respectively. The estimated Doppler scale values are more scattered with sampling rate of 10 compared to 50.

Fig. 11 and 12 illustrates the coarse estimated Doppler scale in a 50m channel using only the first channel tap for 10 times and 50 times the original sampling rate respectively. The estimated Doppler scale values are more scattered with sampling rate of 10 compared to 50.

Ideally, estimation with 3 taps should provide better accuracy. At the same time higher number of taps inject more noise in the estimation calculation. In the above figures it can be seen that compared to estimation with 3 taps, estimation with 1 tap gives less scattered values in both sampling rate situations.

The estimated values in 100m channel using 3 taps and 10 times sampling rate is more scattered compared to the corresponding values in 50m channel. The estimated values in 100m channel using 1 tap and 50 times sampling rate is more scattered compared to the corresponding values in 50m channel.

Fig. 15 and Fig. 16 illustrate the BER in a 100m channel, where the Doppler scale is estimated using the first 3 channel taps with sampling rate of 10 and the data signal is sampled 1000 times the sampling rate. Fig. 17 and 18 illustrate the BER in a 100m channel, where the Doppler scale is estimated using the first 3 channel taps with sampling rate of 50 and the data signal is sampled 1000 times the sampling rate. In the above BER figures, the estimation is done with a sampling rate of 10 and 50. But to show how Doppler compensation works, data is sampled at 1000, so even after the rounding of sample index, some Doppler scale values cause Doppler shift and hence Doppler distortion. For these effective Doppler scale shifts, when the data samples are shifted back with the exact Doppler scale values, they show BER performance similar to the case without Doppler. However when, the estimated Doppler scale values are used to resample, some of the BER plots return to no Doppler state but others are not fully compensated and hence the BER performance is not good for those Doppler scales.

B. Simulation Using Second Algorithm

Fig. 13 and 14 illustrates the coarse estimated Doppler scale in a 100m channel using the first 3 channel taps for 10 times and 50 times the original sampling rate respectively.

During estimation and data sampling, when the rate is 10 or 50, the Doppler shifted samples are not hit because of low sampling rate and because of rounding the indexes during simulation. So, even though there is Doppler shift, the effect is not seen in the above BER plots, that is Doppler absence and presence act the same way.

Fig. 19 and Fig. 20 illustrate the BER in a 100m channel, where the Doppler scale is estimated using the first 3 channel taps with sampling rate of 10 and the data signal is sampled 1000 times the sampling rate. Fig. 21 and 22 illustrate the BER in a 100m channel, where the Doppler scale is estimated using the first 3 channel taps with sampling rate of 50 and the data signal is sampled 1000 times the sampling rate. In the above BER figures, the estimation is done with a sampling rate of 10 and 50. But to show how Doppler compensation works, data is sampled at 1000, so even after the rounding of sample index, some Doppler scale values cause Doppler shift and hence Doppler distortion. For these effective Doppler scale shifts, when the data samples are shifted back with the exact Doppler scale values, they show BER performance similar to the case without Doppler. However when, the estimated Doppler scale values are used to resample, some of the BER plots return to no Doppler state but others are not fully compensated and hence the BER performance is not good for those Doppler scales.

In comparison to the first method, the second estimation method performs worse. The estimated Doppler scale values deviate far from the actual values compared to the first estimation method. This is due to the fact that in the second estimation method, noisy data symbol is autocorrelated in addition to the cross correlation of reference OFDM symbol leading to more noise in the calculation.

VI. Conclusion and Future Research

Doppler shift in frequency domain is caused by time selectivity of UAC channels in time domain. This Doppler shift

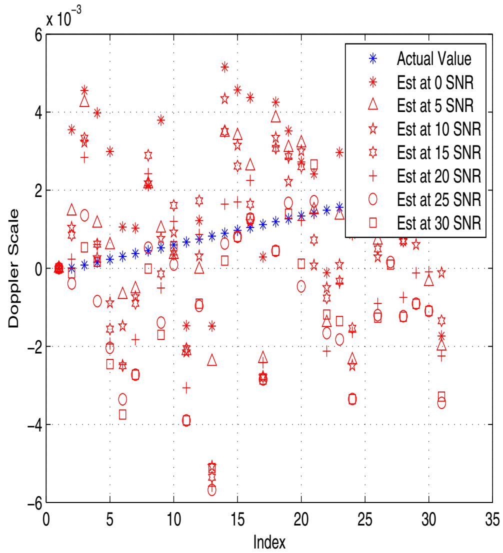

Fig. 5: First Estimation Method, Channel 100m, Taps 3, Rate 10

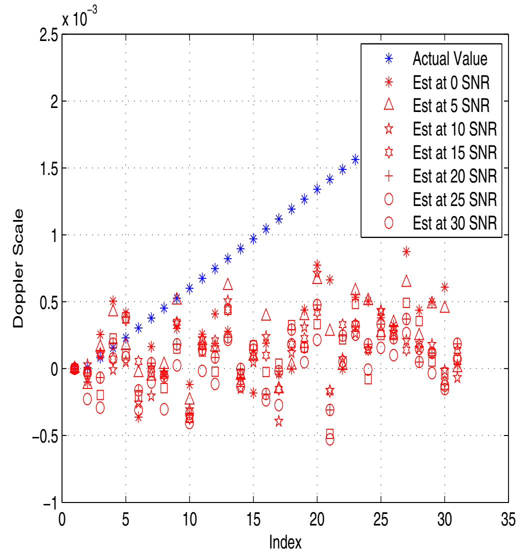

Fig. 6: First Estimation Method, Channel 100m, Taps 3, Rate 50

varies considerably over OFDM subcarriers in UAC OFDM causing ICI and subsequently loss of orthogonality that may degrade receiver performance.

The variation of Doppler shift over OFDM subcarriers can be represented with Doppler scale in time domain. In this paper, two Doppler scale estimation methods are proposed. In both methods, one known reference OFDM symbol is transmitted prior to the data symbols. The known reference is cross correlated with the known local symbol at the receiver. In the first method, with respect to the known tap locations the cross correlated peak locations give a coarse estimation of the Doppler scale. In the second method, the cross correlated peaks of the reference are compared to the auto correlated peaks of a data symbol to provide estimation of the Doppler scale. Between these two methods, first one provides more estimation accuracy since clean reference is used without usage of noisy data symbol. In the first method, the knowledge of the channel taps in the absence of Doppler is needed. In the second method, although this prior knowledge is not necessary, the noise from the auto correlated noisy data contribute to more noise in estimation.

As a continuation of this research in the future, strong code selection in the reference OFDM, which is robust against UAC channels to reduce estimation error can be investigated.

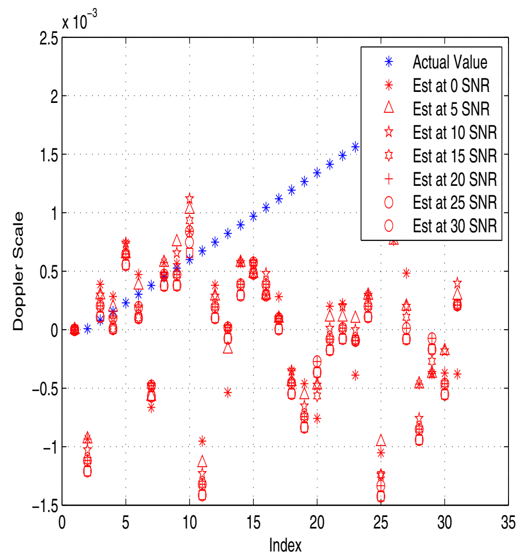

Fig. 7: Doppler Scale, First Estimation Method, Channel 100m, Taps 1, Rate 10

REFERENCES

[1] A. Salberg and A. Swami, “Doppler and frequency-offset synchronization in wideband OFDM: Estimators and performance analysis,” *Proc. Nordic Signal Processing (NORSIG)*.

[2] B. Li, S. Stojanovic, M. Freitag, and P. Willett, “Non-Uniform Doppler Compensation for Zero-Padded OFDM over Fast-Varying Underwater Acoustic Channels,” *proc. MTS/IEEE OCEANS*, pp. 1–6, 2007.

[3] S. Mason, C. Berger, S. Zhou, and P. Willett, “Detection, synchronization, and Doppler scale estimation with multicarrier waveforms in underwater acoustic communication,” *Selected Areas in Communications, IEEE Journal on*, vol. 26, no. 9, pp. 1638–1649, 2008.

[4] B. Li, S. Zhou, M. Stojanovic, L. Freitag, and P. Willett, “Multicarrier communication over underwater acoustic channels with nonuniform Doppler shifts,” *Oceanic Engineering, IEEE Journal of*, vol. 33, no. 2, pp. 198–209, 2008.

[5] C. Berger, S. Zhou, J. Preisig, and P. Willett, “Sparse channel estimation for multicarrier underwater acoustic communication: From subspace methods to compressed sensing,” *Signal Processing, IEEE Transactions on*, vol. 58, no. 3, pp. 1708–1721, 2010.

[6] Stojanovic, “Low Complexity OFDM Detector for Underwater Acoustic Channels,” *Oceans*, pp. 1–6, Sep 2006.

[7] M. Stojanovic, “Recent advances in high-speed underwater acoustic communications,” *Oceanic Engineering, IEEE Journal of*, vol. 21, no. 2,

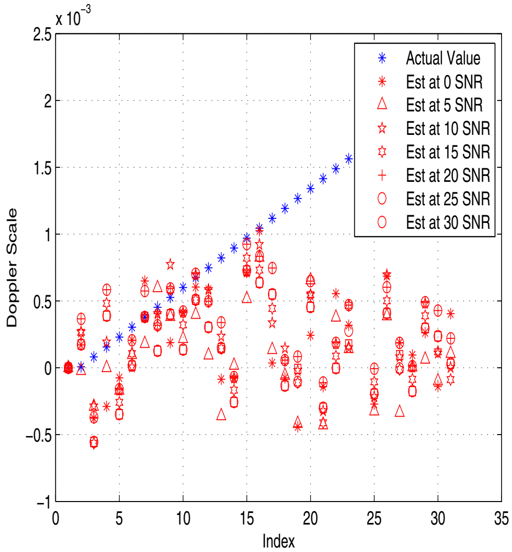

Fig. 8: Doppler Scale, First Estimation Method, Channel 100m, Taps 1, Rate 50

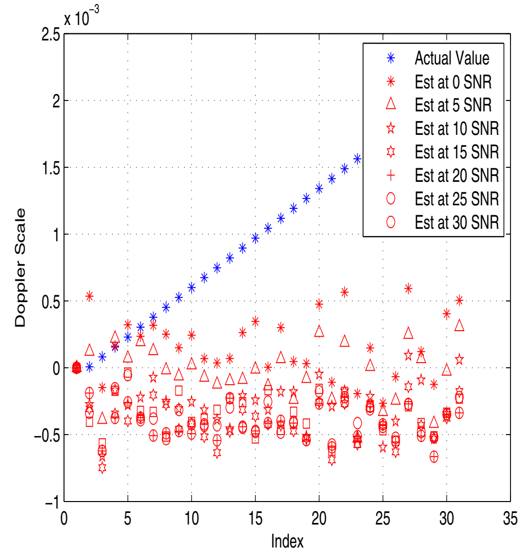

Fig. 10: First Estimation Method, Channel 50m, Taps 3, Rate 50

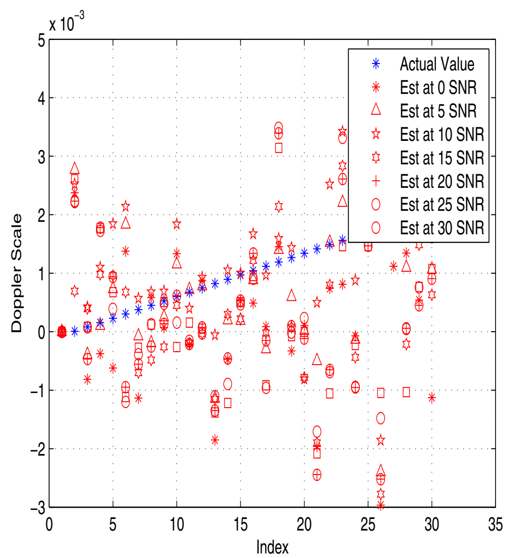

Fig. 9: First Estimation Method, Channel 50m, Taps 3, Rate 10

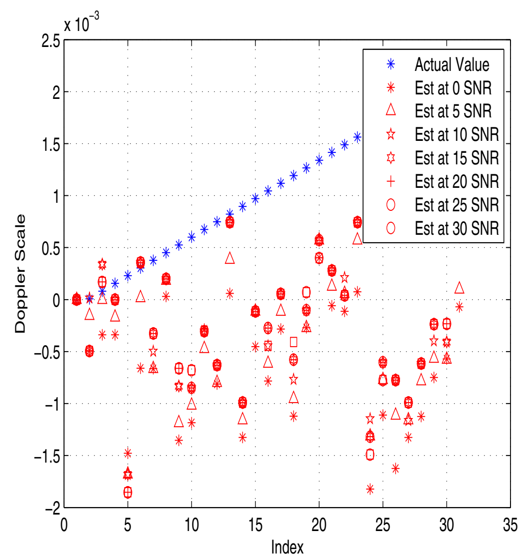

Fig. 11: First Estimation Method, Channel 50m, Taps 1, Rate 10

pp. 125–136, 1996.
[8] B. Kim and I. Lu, "Parameter study of OFDM underwater communications system," in *proc. MTS/IEEE OCEANS*, vol. 2, 2000.
[9] J. Huang, S. Zhou, J. Huang, R. C. Berger, and P. Willett, "Progressive inter-carrier interference equalization for ofdm transmission over time-varying underwater acoustic channels," *IEEE J. Selected Topics in Signal Processing*, vol. 5, no. 8, pp. 1524–1536, Dec. 2011.
[10] T. Kang and R. Iltis, "Iterative carrier frequency offset and channel estimation for underwater acoustic OFDM systems," *Selected Areas in Communications, IEEE Journal on*, vol. 26, no. 9, pp. 1650–1661, 2008.
[11] W. Lam, R. Ormondroyd, and J. Davies, "A frequency domain adaptive coded decision feedback equalizer for a broadband UWA COFDM system," in *OCEANS'98 Conference Proceedings*, vol. 2. IEEE, 2002, pp. 794–799.
[12] Z. Wang, S. Zhou, B. G. Giannakis, R. C. Berger, and J. Huang, "Frequency-domain oversampling for zero-padded ofdm in underwater acoustic communications," *IEEE J. Oceanic Engineering*, vol. 37, no. 1, pp. 14–24, Jan. 2012.
[13] K. Tu, D. Fertonani, M. T. Duman, M. Stojanovic, G. J. Proakis, and P. Hursky, "Mitigation of intercarrier interference for ofdm over time-varying underwater acoustic channels," *IEEE J. Oceanic Engineering*, vol. 36, no. 2, pp. 156–171, Apr. 2011.
[14] Z. Wang, S. Zhou, J. Catipovic, and J. Huang, "Factor-graph-based joint ibi/ici mitigation for ofdm in underwater acoustic channels with long-separated clusters," *IEEE J. Oceanic Engineering*, vol. 37, no. 4, pp. 680–694, Oct. 2012.
[15] P. Carrascosa and M. Stojanovic, "Adaptive MIMO detection of OFDM signals in an underwater acoustic channel," in *OCEANS 2008*. IEEE,

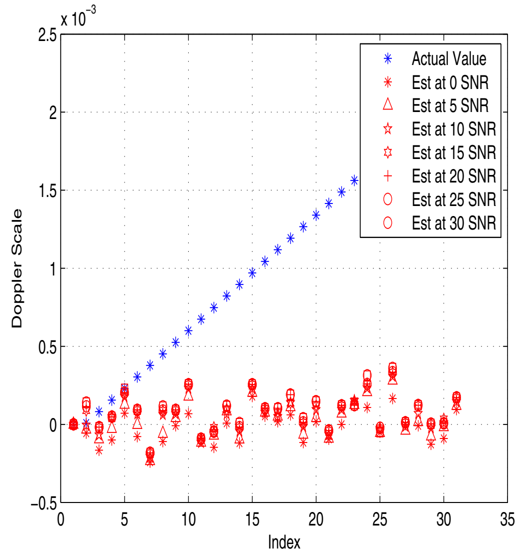

Fig. 12: First Estimation Method, Channel 50m, Taps 1, Rate 50

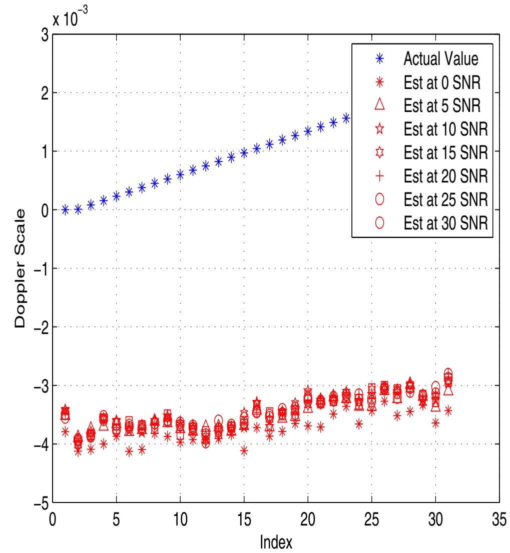

Fig. 14: Second Estimation Method, Channel 100m, Taps 3, Rate 50

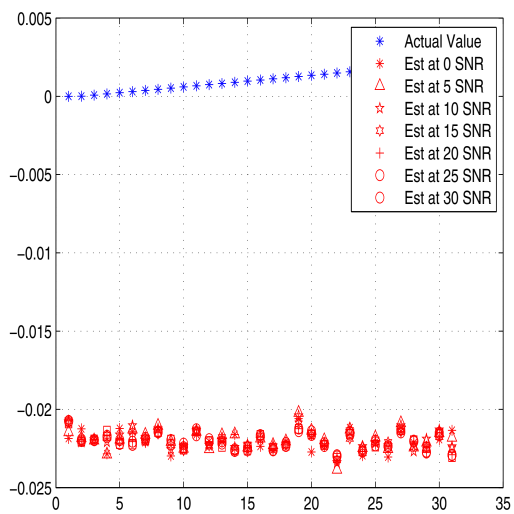

Fig. 13: Second Estimation Method, Channel 100m, Taps 3, Rate 10

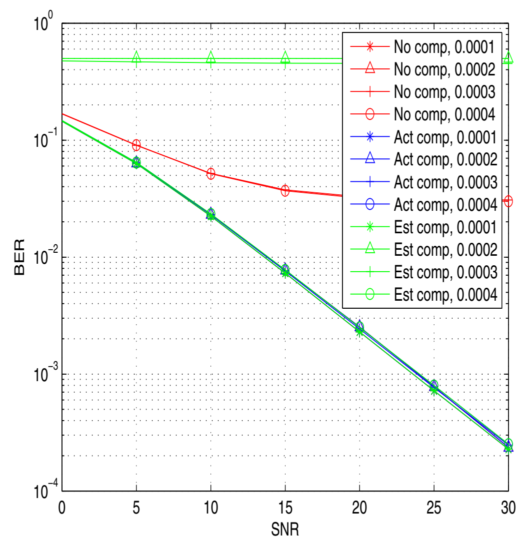

Fig. 15: BER, First Method, Channel 100m, Taps 3, Est. Rate 10, BER Rate 1000, First 4

2009, pp. 1–7.

[16] G. Leus and P. van Walree, "Multiband OFDM for covert acoustic communications," *Selected Areas in Communications, IEEE Journal on*, vol. 26, no. 9, pp. 1662–1673, 2008.

[17] S. Yerramalli and U. Mitra, "Optimal resampling of ofdm signals for multiscale-multilag underwater acoustic channels," *IEEE J. Oceanic Engineering*, vol. 36, no. 1, pp. 126–138, Jan. 2011.

[18] S. Beygi and U. Mitra, "Optimal bayesian resampling for ofdm signaling over multi-scale multi-lag channels," *IEEE Signal Processing Letters*, vol. 20, no. 11, pp. 1118–1121, Nov. 2013.

[19] T. S. Rappaport, *Wireless Communications: principles and practice, Pearson Education, Delhi, India:*. Pearson, 2002, ch. Mobile Radio Propagation: Small-Scale Fading and Multipath, pp. **5**–182 – **5**–183.

[20] I. Capoglu, Y. Li, and A. Swami, "Effect of Doppler spread in OFDM-based UWB systems," *Wireless Communications, IEEE Transactions on*, pp. 2559–2567, Sep 2005.

[21] R. Y. Yen, H. Y. Liu, and W. Tsai, "QAM Symbol Error Rate in OFDM Systems Over Frequency-Selective Fast Ricean Fading Channels," *Vehicular Technology, IEEE Transactions on*.

[22] Y. Mostofi and D. Cox, "ICI Mitigation for Pilot-Aided OFDM Mobile Systems," *Wireless Communications, IEEE Transactions on*, vol. 4, no. 2, pp. 765–774, 2005.

[23] M. Chitre, J. Potter, and O. Heng, "Underwater acoustic channel characterisation for medium-range shallow water communications," *proc. MTS/IEEE OCEANS*, pp. 9–12, Nov 2004.

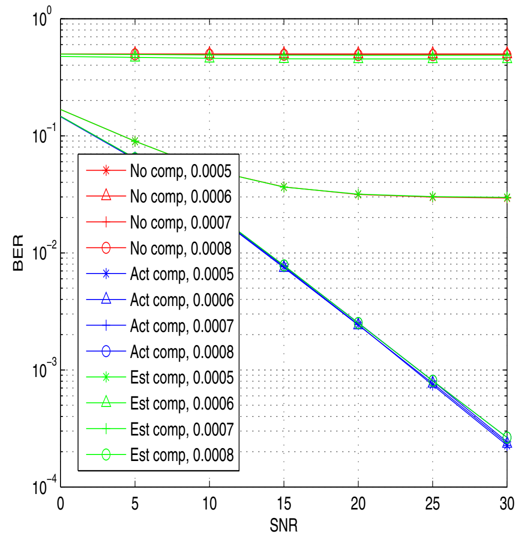

Fig. 16: BER, First Method, Channel 100m, Taps 3, Est. Rate 10, BER Rate 1000, Last 4

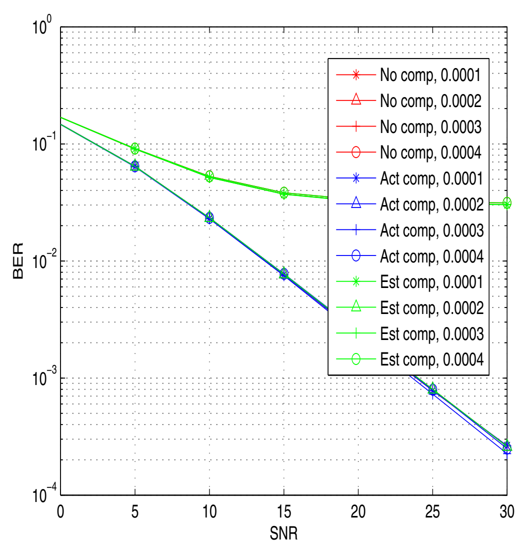

Fig. 17: BER, First Method, Channel 100m, Taps 3, Est. Rate 50, BER Rate 1000, First 4

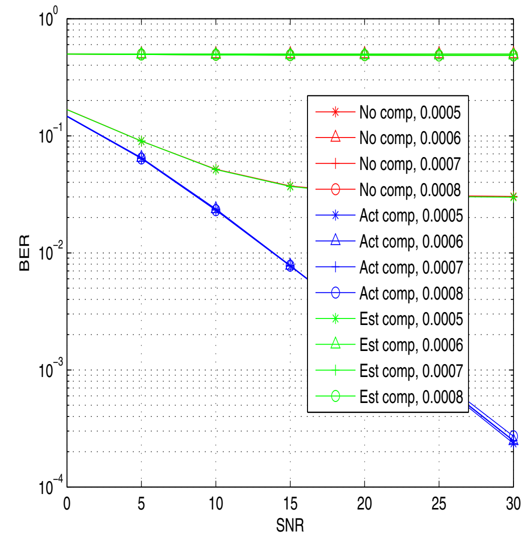

Fig. 18: BER, First Method, Channel 100m, Taps 3, Est. Rate 50, BER Rate 1000, Last 4

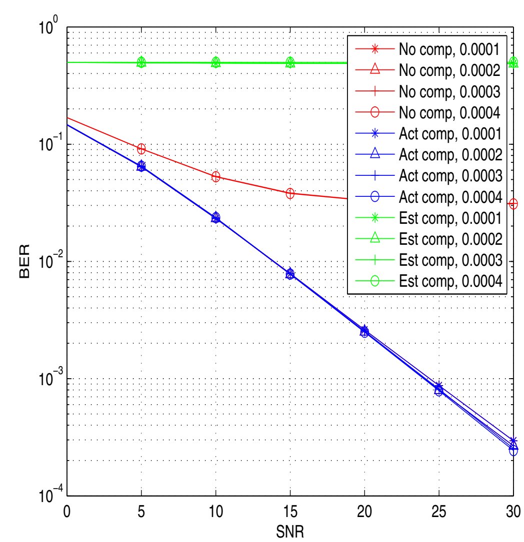

Fig. 19: BER, Second Method, Channel 100m, Taps 3, Est. Rate 10, BER Rate 1000, First 4

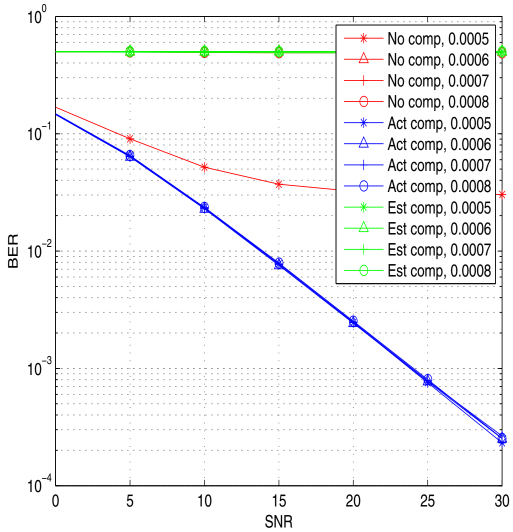

Fig. 20: BER, Second Method, Channel 100m, Taps 3, Est. Rate 10, BER Rate 1000, Last 4

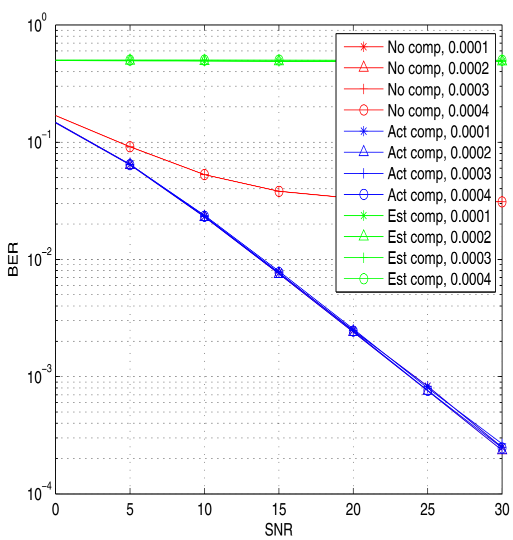

Fig. 21: BER, Second Method, Channel 100m, Taps 3, Est. Rate 50, BER Rate 1000, First 4

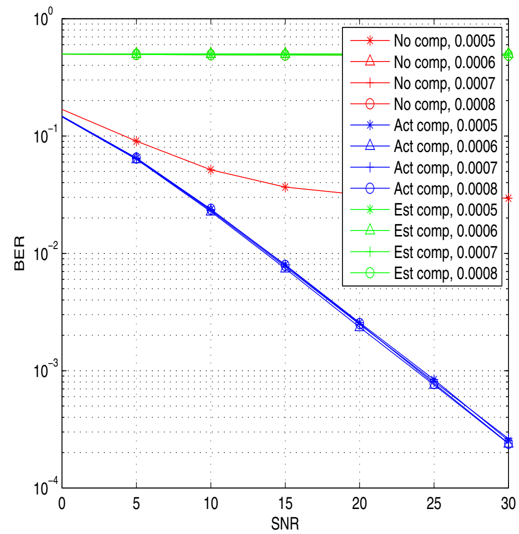

Fig. 22: BER, Second Method, Channel 100m, Taps 3, Est. Rate 50, BER Rate 1000, Last 4